*buildings*

MDPI

*Article*

# Deflection Calculation of Fatigue-Damaged RC Beams Under Chloride Exposure

**Jian Yang, Jieqiong Wu *, Liu Jin and Xiuli Du**

The College of Architecture and Civil Engineering, Beijing University of Technology, Beijing 100124, China; yangjianqingmu@163.com (J.Y.); kinglew2007@163.com (L.J.); duxiuli@bjut.edu.cn (X.D.)
* Correspondence: jieqiong.wu@bjut.edu.cn

**Abstract**

A prediction methodology for the mid-span deflection of fatigue-damaged RC beams subjected to chloride-induced corrosion is proposed, incorporating the coupled effects of fatigue stress levels and localized pitting corrosion in steel reinforcement. The reliability of the methodology is validated through experimental comparisons. The effects of fatigue stress are quantified via two mechanisms: degradation of the concrete elastic modulus and the development of fatigue-induced cracks in the steel reinforcement, which reduces its effective cross-sectional area. Pitting corrosion is simplified as equivalent surface cracks. To determine the chloride concentration within the concrete cover for predicting steel pit depth, a 3D meso-scale model is developed to simulate chloride ingress in fatigue-damaged concrete. The concrete is treated as a three-phase composite composed of coarse aggregate, mortar matrix, and the interfacial transition zone (ITZ), and each phase has its own diffusion coefficient. Based on previous chloride concentration tests, the effect of fatigue loading is considered by the accelerated and depth-dependent diffusion coefficients. Based on the meso-scale simulation results, mid-span deflections of fatigue-damaged RC beams under varying chloride exposure durations are predicted. The findings conclusively demonstrate that, under prolonged chloride erosion, the mechanical stress state remains the predominant factor governing structural deformation, overshadowing time-dependent corrosion effects.

**Keywords:** RC beam; deflection; fatigue damage; corrosion; numerical simulation

check for updates

Academic Editor: Ray Kai Leung Su

Received: 13 November 2025
Revised: 26 November 2025
Accepted: 27 November 2025
Published: 2 December 2025

**Citation:** Yang, J.; Wu, J.; Jin, L.; Du, X. Deflection Calculation of Fatigue-Damaged RC Beams Under Chloride Exposure. *Buildings* **2025**, *15*, 4374. https://doi.org/10.3390/buildings15234374

**Copyright:** © 2025 by the authors. Licensee MDPI, Basel, Switzerland. This article is an open access article distributed under the terms and conditions of the Creative Commons Attribution (CC BY) license (https://creativecommons.org/licenses/by/4.0/).

## 1. Introduction

In coastal areas, reinforced concrete (RC) bridges are continuously subjected to vehicle loads throughout their service life, which can be approximated as fatigue loads [1]. Compared to static loads, fatigue loading induces cracks and stress gradients that significantly accelerate chloride ingress into concrete [2], thereby degrading the mechanical performance of RC structures [3]. Deflection is a critical safety indicator for RC structures, as it directly relates to their load-bearing capacity and resistance to dynamic loads such as earthquakes. Therefore, it is of significant importance to investigate how fatigue-induced deflection degrades in RC beams under chloride attack.

For RC beams subjected to static loading, many design codes, including GB 50010-2010 [4] and ACI 318 [5], have established a deflection calculation theory and a general consensus exists. However, for RC beams subjected to fatigue loading, many studies have been carried out to propose a calculation theory, but the calculation methods lack uniformity. The existing studies have established some methods to analyze the reduction in the stiffness

or deflection of the RC beams [6–8]. Wang et al. [6] conducted fatigue tests on six steel–concrete composite beams and developed a model for predicting the residual stiffness through parameter fitting based on the test results and a stiffness degradation function. Based on the relevant theories of damage mechanics, Zuo et al. [7] proposed a two-stage stiffness degradation model for RC beams considering fatigue cracks, aiming to investigate the effect of stiffness degradation by fatigue loading on the natural frequency of the structure. Li et al. [8] explored the effect of fatigue stress level on stiffness degradation and fatigue life, developing a predictive model based on tests of three continuous beams with prestressed CFRP bars. Eljufout and Toutanji [9] developed an ANSYS model for FRP-strengthened RC beams to investigate the deflection behavior of reinforced concrete beams under fatigue loading. Ultimately, an analytical model was proposed to predict the deflection process of RC beams strengthened with near-surface mounted (NSM) FRP, which has been validated through experimental and numerical simulations, demonstrating an average prediction error of less than 9.5% for deflection. Atutis et al. [10] proposed a deflection prediction method for BFRP-prestressed concrete beams based on a single-degree-of-freedom system and a cyclic creep model of concrete. By integrating structural dynamics with time-dependent material properties, it achieved accurate simulation of beam deflection evolution under fatigue loading. Validated against experimental data from 12 test beams, the model demonstrated a mean deflection prediction-to-experimental ratio of approximately 1.36 with a standard deviation of 0.14, showing superior accuracy and reliability compared to conventional methods.

The effect of chloride-induced corrosion on the deflection of RC beams is also significant. Zhu et al. [11] tested the flexural capacity of RC beams in service for 26 years and the results showed that the loss of cross-sectional area of steel bar due to chloride corrosion had a significant effect on the stiffness of RC beams, which led to large deflection. Zhang et al. [12] used three current densities for the accelerated corrosion of RC beams, followed by fatigue loading, and the results showed that electrically accelerated corrosion exacerbated the bond damage, leading to a reduction in the stiffness of the RC beams. Furthermore, several studies have investigated the coupled effect of fatigue loading and chloride corrosion on the deflection-predicted models of RC beams. Huang et al. [13] established a method for calculating the stiffness and deflection of corroded prestressed concrete, which considers the stress redistribution between prestressed steel strands and steel bars, the fatigue damage of concrete, and the corroded steel bars with fatigue damage. Zhang et al. [14] proposed a deflection calculation method for T-shaped RC beams that incorporates the number of fatigue loadings, stress amplitude, degradation of concrete elastic modulus, and reinforcement corrosion. Based on the experimental results of RC beams subjected to both imposed displacements/cyclic loading and accelerated corrosion, Dackman et al. [15] proposed a model for characterizing corrosion propagation through corrosion-induced deflection. The model utilizes strain measurements from distributed optical fiber sensors to compute time-dependent deflections and crack patterns, enabling corrosion development evaluation based solely on measured deflections.

In actual engineering, the corrosion of steel bars in concrete structures is non-uniform [16,17]; that is, the steel bars on the side closer to the protective layer are more severely corroded and there are local corrosion phenomena such as pitting corrosion [18]. In the chloride environment, pitting corrosion in steel bars is more common and dangerous, causing almost 70% of corrosion damage compared with uniform corrosion [19,20]. However, the corrosion rate of the reinforcement of RC beams is difficult to obtain in practice, while much research has shown that the corrosion rate is related to the chloride concentration within the concrete cover [21,22]. Numerous studies have employed numerical simulation to investigate chloride ingress in concrete [23–25]. Oh and Jang [23] proposed

a simple analytical model to predict the chloride diffusion coefficient of concrete, which considers the microstructural properties of the cement paste, such as the capillary porosity, pore structure parameters, solid-phase diffusivity, aggregate volume fractions, and interfacial transition zone (ITZ) properties. Du et al. [24] established a meso-scale model treating concrete as a three-phase composite and analyzed the influence of the aggregate distribution, shape, water–cement ratio, and content on chloride ingress. Based on the elasticity theory, Xu and Li [25] proposed an analytical model to investigate the chloride ingress in concrete and explored the quantitative relationships between the external equivalent stress and chloride diffusion coefficients, mortar porosity, and ITZ.

Therefore, this study aims to establish a deflection calculation model for RC beams that incorporates the combined effects of fatigue loading and pitting corrosion. Based on the previous studies [26], the deflection of beam specimens under fatigue loading typically follows a three-stage pattern: a rapid initial increase, a prolonged slow growth phase until about 90% of the fatigue life, and a final stage of rapid failure. The deflection calculation model, in this study, focuses on the second stage. In addition, a 3D meso-scale model is developed to simulate the chloride ingress in fatigue-damaged concrete, and the reliability of the model is verified. According to the simulation results, the deflection of the fatigue-damaged RC beams with fatigue loading after 10, 20, 40, and 60 years of chloride exposure is predicted.

## 2. Experimental Test

### *2.1. Experimental Description*

In our previous studies [27–30], twelve RC beam specimens with the same dimension (Figure 1) were manufactured to explore the effect of fatigue stress and chloride corrosion on mid-span deflections. The twelve beam specimens were divided into two groups. Group A beam specimens (A1, A2, A3, and A4) were subjected to fatigue loading under atmospheric conditions (i.e., without the chloride exposure). Group B beam specimens (B1–B8) were subjected to 0.4 million cycles of fatigue loading, as detailed in Table 1. After the initial loading, B1–B4 beam specimens were exposed to 3 months of 3.5% NaCl solution wet–dry cycles, while B5–B8 were exposed to 6 months. Specifically, each cycle consisted of 6 h of full immersion, with all six surfaces exposed to the NaCl solution, followed by 42 h of air drying. Then, after 3 or 6 months of the exposure, the beam specimens were fatigue loaded again until failure or the number of loading cycles reached 5.4 million. Subsequently, the average chloride concentration was measured at three locations within the 40 mm depth of concrete in the middle section of beam specimens B5–B8, which has been detailed in our previous work [31]. In this study, the effect of the existence of steel bars on the chloride ingress is not incorporated. The method of the chloride concentration measurements refers to the study of Li et al. [32].

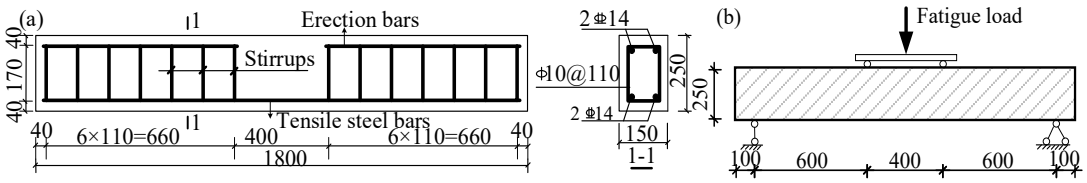


**Figure 1.** Specimen and loading device: (**a**) RC beam reinforcement diagram and (**b**) loading device diagram.

**Table 1.** Experimental parameters of RC beams.

| Beam | Initial Loading Number | Exposure Time | $\sigma_{s,max}$ (MPa) | $a_{sc}$ (mm) | Fatigue Loads (kN) | | Fatigue Life $N$ | $C_{steel}$ ($10^{-2}$%) | $S_{max}$ |
|---|---|---|---|---|---|---|---|---|---|
| | | | | | Maximum | Minimum | | | |
| A1 | - | - | 128 | 1.24 | 24 | 6 | >5,000,000 | - | 0.28 |
| A2 | - | - | 192 | 0.42 | 36 | 6 | >5,000,000 | - | 0.43 |
| A3 | - | - | 256 | 0.21 | 48 | 6 | 4,490,000 | - | 0.57 |
| A4 | - | - | 293 | 0.17 | 55 | 6 | 970,000 | - | 0.65 |
| B1 | 0.4 million | 0.25 years | 128 | 1.24 | 24 | 6 | >5,400,000 | 2.30 | 0.28 |
| B2 | 0.4 million | 0.25 years | 192 | 0.42 | 36 | 6 | - | 2.40 | 0.43 |
| B3 | 0.4 million | 0.25 years | 256 | 0.21 | 48 | 6 | 2,710,000 | 2.90 | 0.57 |
| B4 | 0.4 million | 0.25 years | 293 | 0.17 | 55 | 6 | 770,000 | 3.20 | 0.65 |
| B5 | 0.4 million | 0.5 years | 128 | 1.24 | 24 | 6 | >6,000,000 | 1.60 | 0.28 |
| B6 | 0.4 million | 0.5 years | 192 | 0.42 | 36 | 6 | >6,000,000 | 1.90 | 0.43 |
| B7 | 0.4 million | 0.5 years | 256 | 0.21 | 48 | 6 | 573,452 | 3.87 | 0.57 |
| B8 | 0.4 million | 0.5 years | 320 | 0.15 | 60 | 6 | 169,372 | 4.20 | 0.71 |

Note: $\sigma_{s,max}$ is the maximum stress of the tensile steels; $a_{sc}$ is the threshold crack size of the steel bar caused by fatigue loading; $C_{steel}$ is the chloride concentration at the steel bar surface; $S_{max}$ is the ratio of the maximum stress over the ultimate strength for the tensile steels, i.e., the stress level.

### *2.2. Experimental Results*

According to the previous study [26], the complete fatigue loading was composed of initial fatigue loading and fatigue life test, and the total deflection at mid-span can be expressed as

$$D = \Delta D + D_r \quad (1)$$

where $\Delta D$ is the deflection (mm) caused by the fatigue life test; $D_r$ is the deflection caused by initial fatigue loading, and $D_r$ is zero for Group A beam specimens.

Figure 2 presents the relationship between the deflection increment and total deflection versus cycle ratio ($N/N_f$) for Group A and B beam specimens. As shown in Figure 2, the fatigue stress level significantly influences both the deflection increment and total deflection, irrespective of the chloride exposure. Moreover, chloride corrosion exacerbates the effect of the fatigue stress level. As detailed in Figure 2a, the deflection increment of specimen B4 ($S_{max}$ = 0.65) is 1.68 times that of specimen B1 ($S_{max}$ = 0.28) and 1.37 times that of specimen B3 ($S_{max}$ = 0.57). This corresponds to a 23% growth in the deflection increment as the fatigue stress level rises from 0.28 to 0.57 and a further 37% growth as it increases from 0.57 to 0.65. Furthermore, for Group A specimens (without chloride corrosion), the deflection increments of A1 to A4 (with fatigue stress levels from 0.28 to 0.65) exhibit apparent differences, ranging from approximately 0.3 mm to 0.8 mm. Meanwhile, Figure 2a indicates that, under the same fatigue stress level, the deflection increments of Group B are smaller than those of Group A. This is primarily attributed to the plastic deflection caused by the initial fatigue loading and the deposit filling or the self-healing of the cracks during chloride exposure. However, as depicted in Figure 2b and quantified through Equation (1), the total deflection of Group B significantly exceeds that of Group A.

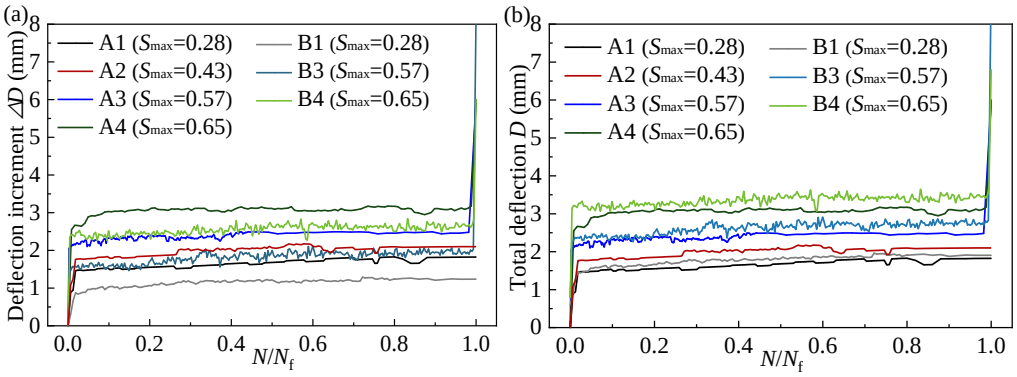


**Figure 2.** Deflection increment and total deflection of Group A and B beam specimens: (**a**) deflection increment and (**b**) total deflection ($N$ is the fatigue cycle in the test, $N_f$ is the fatigue life).

## 3. The Deflection Calculation of Fatigue-Damaged RC Beams Under Chloride Attack

### *3.1. The Determination of Deflection for RC Beams*

Based on the classical principle of mechanics, the deflection of the RC beam can be expressed as

$$D = \zeta \frac{Ml^2}{B}, \tag{2}$$

where $D$ is the mid-span deflection of the RC beam, i.e., the total deflection in Section 2.2; $\zeta$ is the deflection coefficient affected by the supporting conditions and load forms; for a simply supported beam with the shear span, symmetrically loaded at two points, the $\zeta = [3 - 4(a^2/l2)]/24$; $l$ is the calculated span of the beam; $B$ is the bending stiffness of the beam. The short-term stiffness ($B_s$) of RC beams subjected to the fatigue loading can be expressed as [33]

$$B_S = \frac{E_S A_S h_0^2}{1.35 + 6\phi_E \rho}, \tag{3}$$

$$\phi_E = \frac{E_s}{E_c}, \tag{4}$$

where $E_s$ and $E_c$ are the elasticity modulus of the steel bar and concrete, respectively; $A_s$ is the effective cross-sectional area of the longitudinal steel bars; $h_0$ is the effective height of the beam section; $\phi_E$ is the ratio of the elasticity modulus of steel bar and concrete; $\rho$ is the longitudinal reinforcement ratio. The stiffness considering the long-term action can be determined by [33]

$$B = \frac{B_s}{\theta}, \tag{5}$$

where $\theta$ is the stiffness correction coefficient considering the effect of the long-term action of the loads, which is related to the reinforcement ratios for tensile and compressive steel bars. Due to the absence of the compressed steel bar in RC beams, $\theta$ is taken as 1.6 in this study.

### *3.2. The Influence of Pit Corrosion and Fatigue Loading on Deflection*

It is widely recognized that the tensile steel bar governs the failure of RC beams under fatigue loading in most cases [34]. As indicated by Equations (2) and (3), the cross-sectional area of the steel bar significantly influences the deflection of RC beams. In this study, the reduction in this area is attributed to two primary mechanisms: chloride attack and fatigue loading.

In this study, chloride attack is considered to be pitting corrosion, which is treated as a surface crack for simplification. The pitting corrosion caused by the chloride in concrete is an electrochemical process, and the corrosion pit depth is as follows.

$$a_{\mathrm{cor}}(t) = 0.0116\tau \int i dt, \tag{6}$$

where $a_{\mathrm{cor}}$(t) is the corrosion pit depth (mm) when the time is $t$ (s); $\tau$ is the ratio of maximum pit corrosion depth to the uniform corrosion depth; $i$ is the corrosion rate ($\mu A/cm^2$). The corrosion rate $i$ is influenced by the chloride ingress, which can be calculated by Equation (7) in GB 50476-2019 [4]. It is noted that modeling pits as simplified cracks does not capture the intricate geometry and localized stress concentrations of real pitting corrosion. However, this approach is justified for predicting the macroscopic beam deflection, as the dominant mechanism is the reduction in the steel bar's effective cross-sectional area, which governs the overall bending stiffness.

$$\ln i = 8.617 + 0.618 \ln C_{\mathrm{s}} - \frac{3034}{T + 273} - 5 \times 10^{-3}[11.1(1.8 - C_{\mathrm{c}}) + 10(RH - 1)^2 + 4] + \ln m_{\mathrm{c}} \tag{7}$$

where $C_{\mathrm{s}}$ is the concrete surface chloride concentration ($kg/m^3$); $T$ is the temperature (°C) around the steel bar, for which one can use the atmospheric ambient temperature; $C_{\mathrm{c}}$ is the average value of chloride concentration within concrete cover ($kg/m^3$), and the value of $C_{\mathrm{c}}$ should no more than 3.6; $RH$ is the environmental relative humidity; $m_{\mathrm{c}}$ is the local environmental factor, which is 4.5–5.5 in wet–dry environments.

Directly measuring the average chloride concentration within the concrete cover of fatigue-damaged RC beams is challenging in practice. Thus, the numerical simulation is adopted to investigate the chloride ingress in concrete, which will be detailed in Section 3.3.

Under fatigue loading, steel bars in RC beams develop fatigue cracks, which reduce their effective cross-sectional area. According to a previous study [35], a significant portion of the fatigue life of steel bars in RC beams is consumed during the stage from initial crack development to the threshold crack size ($a_{\mathrm{sc}}$). Thus, it is assumed that at the end of the second stage of deflection development, the depth of the fatigue crack in the steel bar is $a_{\mathrm{sc}}$, which can be determined by

$$a_{\mathrm{sc}} = \frac{(\Delta K_{\mathrm{th}}/SY)^2}{\pi}, \tag{8}$$

$$\Delta K_{th} = 7(1 - 0.85R), \tag{9}$$

$$R = \frac{\sigma_{\mathrm{s,m}in}}{\sigma_{\mathrm{s,max}}}, \tag{10}$$

$$Y = \frac{1.121 - 3.08(a_0/d_0) + 7.344(a_0/d_0)^2 - 10.244(a_0/d_0)^3 + 5.85(a_0/d_0)^4}{\left[1 - 2(a/d_0)^2\right]^{3/2}}, \tag{11}$$

where $\Delta K$th is the threshold of the stress intensity factor (MPa·$\sqrt{m}$); $S$ is the stress range (MPa); $Y$ is a geometry correction factor; $R$ is the stress ratio; $\sigma_{\mathrm{s,max}}$ and $\sigma_{\mathrm{s,min}}$ are the maximum and minimum stress of the tensile steels, respectively.

The development process of steel bar cracks caused by fatigue loads from initial cracks (i.e., the corrosion pit depth) to threshold cracks is assumed to be linear. Thus, the crack depth caused by fatigue loading can be expressed as

$$a_{\mathrm{fatigue}} = \frac{N}{N_{\mathrm{f}}}(a_{\mathrm{sc}} - a_{\mathrm{cor}}). \tag{12}$$

It should be noted that the development of steel bar cracks under fatigue loading is assumed to follow a linear progression from the initial pit depth to the threshold crack size

(Equation (12)). Although the actual fatigue–corrosion processes may be nonlinear, the key coupling with chloride exposure in this model is captured nonlinearly through the pitting corrosion model. Based on our previous study [31], the fatigue life of RC beams under chloride attack can be determined by the fatigue stress level and the chloride concentration level as follows:

$$\begin{cases} \lg N = -9.58\lg S_{max} - 2.34\lg\mu + 4.50 \\ S_{max} = \sigma_{max}/f_y \\ \mu = C_{steel}/C_{ini} \end{cases}, \quad (13)$$

where $\mu$ is defined as the chloride concentration level; $C_{steel}$ is the chloride concentration at the steel bar surface, $C_{steel}$ is taken as zero for the RC beam without chloride attack; $C_{ini}$ is the initial chloride concentration in concrete without chloride attack (the chloride concertation in aggregate and sand during the beam manufacturing).

Figure 3 shows the effective cross-sectional area of the steel bar after corrosion, and the pit depth ($a$) is the sum of the corrosion pit depth ($a_{cor}$) and fatigue crack depth ($a_{fatigue}$):

$$a = a_{fatigue} + a_{cor}. \quad (14)$$

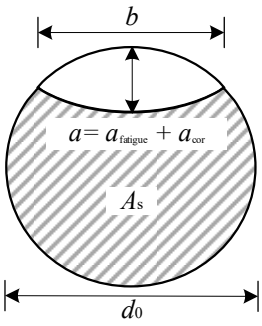


**Figure 3.** The cross-sectional area of steel bar after corrosion.

The pit width can be determined by the pit depth and steel bar diameter, as given in Equation (15) [36,37]:

$$b = 2a\sqrt{1 - \left(\frac{a}{d_0}\right)^2}, \quad (15)$$

where $b$ is the pit width (mm); $a$ is the pit depth (mm); $d_0$ is the steel bar diameter (mm).

The effective cross-sectional area of corroded steel bar Ac can be obtained as follows:

$$A_s = \begin{cases} \pi d_0^2/4 - A_1 - A_2, & a \le \sqrt{2}d_0/2 \\ A_1 - A_2, & \sqrt{2}d_0/2 < a < d_0 \\ 0, & a > d_0 \end{cases} \quad (16)$$

$$A_1 = \frac{1}{2}\left[2arcsin\left(\frac{b}{d_0}\right) \times \left(\frac{d_0}{2}\right)^2 - b\left|\frac{d_0}{2} - \frac{a^2}{d_0}\right|\right], \quad (17)$$

$$A_2 = \frac{1}{2}\left[2arcsin\left(\frac{b}{2a}\right) \times a^2 - b\frac{a^2}{d_0}\right]. \quad (18)$$

The loss rate of the cross-sectional area for corroded steel bars is

$$\eta_{sec} = \frac{A_0 - A_c}{A_0}, \quad (19)$$

$$A_s = A_0 \cdot (1 - \eta_{sec}), \quad (20)$$

where $A_0$ is the cross-sectional area of the steel bar without corrosion.

During the corrosion process, the volumetric expansion of steel corrosion products exerts expansive pressure on the surrounding concrete. Rust expansion cracks appear in the concrete cover, which leads to the reduction in the concrete section and thus changes the effective height of the section. The effective height of the section considering the effect of corrosion can be expressed as

$$h_0' = h_0 - w_{\max}. \tag{21}$$

The relationship between the maximum rust expansion crack and the mass loss rate of steel bar is [38]

$$w_{\max} = \frac{e^{(\eta_{\text{mass}}/0.03)}}{19}. \tag{22}$$

The corrosion rate of the steel bar in Equation (22) is the mass loss rate, and the relationship between the mass loss rate and cross-sectional area loss rate of the steel bar is as follows [39]:

$$\eta_{\text{mass}} = 0.9\eta_{\text{sec}}. \tag{23}$$

According to the study of Holmen [40], the elasticity modulus of concrete attenuates with the accumulation of damage caused by fatigue loading, and the relationship between the elasticity modulus of concrete and fatigue cycles can be expressed as

$$E_N = (1 - 0.33 \times \frac{N}{N_f}) \times E_0, \tag{24}$$

where $E_N$ is the elasticity modulus of concrete after $N$ times of fatigue loading; $E_0$ is the elasticity modulus of concrete without fatigue loading.

Based on the Equations (2)–(24), the deflection of fatigue-damaged RC beam with pitting corrosion can be determined by

$$D = \frac{\zeta\theta M l^2[1.35 + 6\rho \cdot (E_s/E_c)]}{E_s A_s h_0'^2}. \tag{25}$$

Based on our previous study [26], a coefficient of the fatigue stress level on the deflection of RC beams is proposed, as shown in Figure 4, to roughly estimate the deflection of an RC beam when a deflection of the beam at a certain fatigue stress level is obtained.

$$\lambda = 0.005e^{7.7S_{\max}} + 1 \tag{26}$$

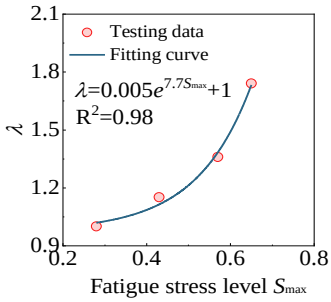


**Figure 4.** Coefficient of fatigue stress level on deflection.

### *3.3. Numerical Simulation of Chloride Ingress in Fatigue-Damaged Concrete*

#### 3.3.1. Mesoscale Model

A three-dimensional (3D) mesoscale model is developed to simulate the chloride ingress into fatigue-damaged concrete in this study, as described in Figure 5. The 3D model is divided into one layer every 10 mm along the height direction of the model (i.e., the $y$-axis direction), to consider the influence of the fatigue damage on the chloride ingress. In

addition, since the previous work [31] proved that the pure flexural segment, i.e., 400 mm in the mid-span, dominates the fatigue failure of the above beams, the cross section with a length of 400 mm is modeled in this study.

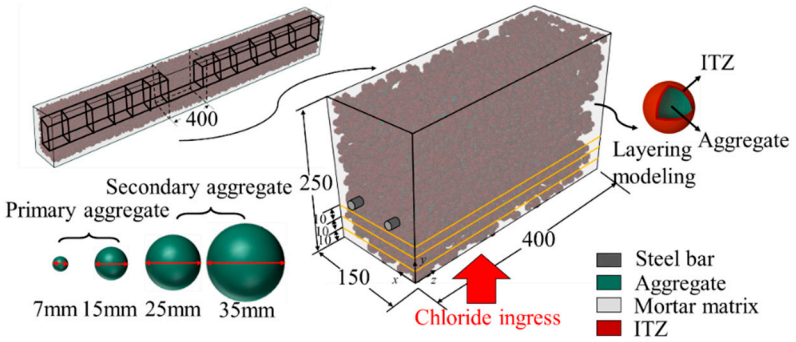


**Figure 5.** Three-dimensional meso-scale model for the chloride ingress into fatigue-damaged RC beams.

The concrete is considered to be a three-phase composite consisting of coarse aggregates, mortar matrix (including fine aggregates with particle size less than 5 mm), and an interfacial transition zone (ITZ) in this study [41]. Therefore, if only coarse aggregates larger than 5 mm in diameter are considered, the aggregate content in concrete is about 35%, and two-graded concrete was adopted, i.e., the diameters of the aggregates were between 5 mm and 40 mm. According to Fuller's curve, the model adopted the equivalent aggregates with diameters of 7 mm and 15 mm to represent aggregates between 5 mm and 20 mm, and the equivalent aggregates with diameters of 25 mm and 35 mm to represent aggregates between 20 mm and 40 mm, as listed in Table 2. In addition, the coarse aggregate particles (indicated by the green area in Figure 5) were randomly placed into the mortar matrix using the classical "pick-and-place" method. The thin layer around the coarse aggregate was set as an interface transition zone with a thickness of 1 mm (indicated by the red area in Figure 5). The mesh of the meso-scale model was set to be 1 mm.

**Table 2.** Aggregate particle size.

| Size Range of Aggregate | 0 mm–5 mm | 5 mm–20 mm | 20 mm–40 mm |
|---|---|---|---|
| Equivalent size | Part of the mortar matrix | 7 mm, 15 mm | 25 mm, 35 mm |

3.3.2. Boundary Conditions

The boundary conditions, including the initial and surface chloride concentration, in all sides of 3D models, are consistent. On the one hand, the initial chloride concentration ($C_{ini}$), which may come from the raw materials used in concrete production, including sand, aggregates, cement, and water, is set at 0.016% according to the tests [31]. On the other hand, the surface chloride concentration ($C_s$) is determined by the measurement value based on Section 2.1 combined with the equations in the study of Song et al. [42], in which the constant and time-dependent surface chloride concentration will be compared. Specifically, in Section 2.1, RC beams have been exposed to the chloride environment for 0.5 years. Consequently, the surface chloride concentration ($C_s$) at 0.5 years can be calculated from the tested chloride profiles within the cover depth based on Fick's second law.

The surface chloride concentration after 0.5 years is determined by the equation recommended by Song et al. [42]:

$$\begin{cases} C_s(t) = C_0 + \alpha \ln(t) \\ t > 1 \end{cases}, \quad (27)$$

where $\alpha$ is a constant value determined as 0.977%/exp(year); t is the time for the concrete exposed by chloride, and the time for the surface chloride concentration to be stable is 5 years [43]; $C_0$ is the initial surface chloride (%/m$^3$), which is regarded as an invariant value within 1 year because of the initial accumulation and which takes the concentration at the exposure time of 0.5 years in this study. The specific values for the surface chloride concentrations ($C_s$) are shown in Table 3.

**Table 3.** Surface chloride concentrations ($C_s$) within 60 years.

| Beam | $S_{max}$ | Time-Dependent $C_s$ (%) | | | | |
|---|---|---|---|---|---|---|
| B5 | 0.3 | 0.5 years | 1.5 year | 2 years | 3 years | |
| | | 0.328 | 0.724 | 1.005 | 1.401 | |
| B6 | 0.4 | 0.5 years | 1.5 year | 2 years | 3 years | |
| | | 0.343 | 0.739 | 1.020 | 1.416 | |
| B7 | 0.55 | 0.5 years | 1.5 years | 2 years | 2.5 years | 3 years |
| | | 0.450 | 0.846 | 1.128 | 1.346 | 1.524 |
| | | 3.5 years | 4 years | 4.5 years | 5 to 60 years | |
| | | 1.674 | 1805 | 1.920 | 2.023 | |
| B8 | 0.7 | 0.5 years | 1.5 years | 2 years | 3 years | |
| | | 0.587 | 0.983 | 1.265 | 1.661 | |

#### 3.3.3. Chloride Diffusion Coefficients

The permeability properties of the mesoscopic components of concrete are determined by their porosity, and hence, each phase holds its own chloride diffusion coefficients, through which the heterogeneity of the concrete can be considered.

##### Concrete Without Fatigue Stress

Compared with the mortar matrix and ITZ, the aggregate is relatively dense with low porosity, and consequently, the diffusion coefficient of the aggregate ($D_{agg}$) is zero. In addition, the mortar matrix can be regarded as a homogeneous medium at the meso-scale [44]. The porosity is a significant factor influencing the chloride diffusion coefficient of the mortar matrix due to the un-hydrated cement particles, hydration products, sand, and the pore network filled with water and air. The porosity is associated with the $w/c$. Therefore, according to the GB/T 21650.1 [45] and ASTM C138/C138M [46], the diffusion coefficient for the mortar matrix ($D_{\text{un-cem}}$) correlates with w/c, as given in the following equation:

$$D_{\text{un-cem}} = [15.93(w/c) - 2.98] \times 10^{-12} \tag{28}$$

The diffusion coefficients of ITZ can be valued as three times the $D_{\text{un-cem}}$ for the concrete without fatigue stress [24]. Thus, the diffusion coefficients for each phase can be summarized as

$$\begin{cases} D_{\text{un-agg}} = 0 \\ D_{\text{un-cem}} = [15.93(w/c) - 2.98] \times 10^{-12} \\ D_{\text{un-ITZ}} = 3 \cdot D_{\text{un-cem}} \end{cases}, \tag{29}$$

where $D_{\text{un-agg}}$ and $D_{\text{un-ITZ}}$ are the chloride diffusion coefficient (m$^2$/s) of aggregates and ITZs, respectively, without fatigue stress.

##### Variation of Chloride Diffusion Coefficient with Time

Treating the chloride diffusion coefficient as a constant has been extensively used in predicting the chloride ingress into concrete based on Fick's second law with a marine

environment [47]. However, the chloride diffusion coefficient decreases over time, since the increasing number of hydration products leads to the increase in the solid hydration fraction in the microstructure and the increase in the complexity of the pore size distribution in the pore area [48]. For accurately predicting the ingress of chloride into concrete, the complexity of chemical substances, cement hydration and chemical reactions between chloride ions, cement, and the other components must be considered to analyze the ingress of chloride into concrete. However, it is typically a complex problem to consider all these factors in chloride ingress analysis. Therefore, considering that the ability of chloride ingress into concrete decreases with time, the modification for the chloride diffusion coefficient is as follows [49]:

$$D_{\text{un-cem}}(t) = D_0\left(\frac{t_0}{t}\right)^m, \tag{30}$$

where $D_{\text{un-cem}}$(t) is the diffusion coefficient of mortar matrix at time t ($m^2/s$); $D_0$ is the diffusion coefficient at $t_0$ ($m^2/s$); $t_0$ is a standard time (28 days) (s); $t$ is the exposed time (s) to chloride; and $m$ is a constant valued as 0.305 based on the concrete mixture in the experimental test [49]. The values for the time-dependent chloride diffusion coefficient within 60 years are shown in Figure 6.

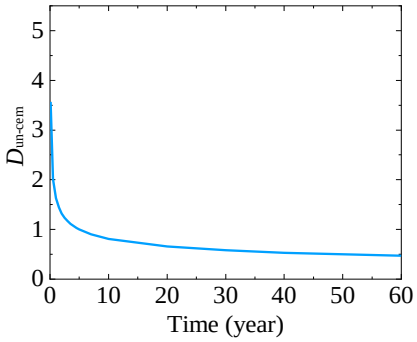


**Figure 6.** Time-dependent chloride diffusion coefficient.

Concrete with Fatigue Stress

Fatigue loading causes fatigue stress in concrete, which is characterized by concrete cracks and the stress gradient [50], as shown in Figure 7a. The effects of both cracks and the stress gradient increase with the increase in the fatigue stress level. For the RC beams, the concrete cracking accelerates the diffusion coefficients in concrete, while the stress inside the concrete decreases when the distance from the beam bottom (i.e., the chloride exposed surface) increases. The diffusion coefficient for concrete is positively correlated with the stress, and consequently, the chloride diffusion coefficient for concrete with fatigue stress is also related to the distance from the chloride-exposed surface. Referring to the literature [49], the influence of fatigue stress is represented by the accelerated and depth-dependent chloride diffusion coefficients to illustrate the effects of concrete cracking and stress gradient, respectively. According to our previous work [31], as shown in Figure 7b, the stress levels ($S_{\max}$) can be applied to represent the concrete damage expressed as $K_\gamma = 0.64 \cdot \exp(1.8 \cdot S_{\max}) + 1$. The depth-dependent diffusion coefficients can be represented by layered modeling along the direction of depth [31], as displayed in Section 3.1, and each layer will be set as a consequential chloride diffusion coefficient.

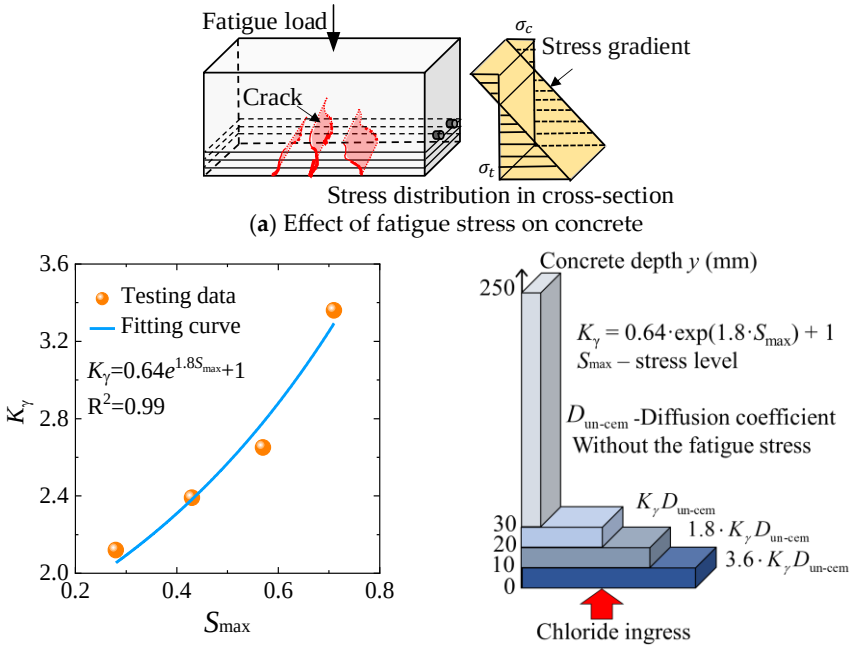


(**a**) Effect of fatigue stress on concrete

(**b**) Fitting curve between Kγ and Smax (**c**) Diffusion coefficients for cement matrix

**Figure 7.** Chloride diffusion coefficient with fatigue stress level.

It is worth noting that, as shown in Figure 7a, in the cross section of the beam specimens, parallel to the fatigue load direction, the chloride diffusion coefficient of concrete is influenced by the cracking and stress gradient. Specifically, for the concrete in the tensile zone, the fatigue stress and the crack width increase when the distance from the neutral axis increases. Hence, the chloride diffusion coefficient decreases with the depth, which is needed to layer the concrete. Meanwhile, in the cross section of the beam specimens, perpendicular to the fatigue load direction, the fatigue stress and the crack width rarely change as the depth varies. Consequently, the chloride diffusion coefficient hardly decreases with the depth, i.e., the model has no need to be layered in this direction.

The accelerated and depth-dependent diffusion coefficients of the concrete with fatigue stress used in the meso-scale model are detailed as follows. Specifically, as shown in Figure 7c, $D_{\text{cem-fatigue}}$ along the direction of depth for concrete is as follows [31,51]:

$$\begin{cases} D_{\text{cem-fatigue}} = D_{\text{un-cem}}, \text{ for } y \geq 30 \text{ mm} \\ D_{\text{cem-fatigue}} = K_\gamma D_{\text{un-cem}}, \text{ for } y = 20 - 30 \text{ mm} \\ D_{\text{cem-fatigue}} = 1.8 \cdot K_\gamma D_{\text{un-cem}}, \text{ for } y = 10 - 20 \text{ mm} \\ D_{\text{cem-fatigue}} = 3.6 \cdot K_\gamma D_{\text{un-cem}}, \text{ for } y = 0 - 10 \text{ mm} \end{cases}, \quad (31)$$

where $y$ is the distance from the concrete surface (mm); $D_{\text{cem-fatigue}}$ is the accelerated $D_{\text{un-cem}}$, considering the concrete cracking and stress gradient [52]. Meanwhile, according to the work of Wu et al. [31], for the concrete with fatigue stress, the $D_{\text{ITZ-fatigue}}$ can also be taken as three times of $D_{\text{cem-fatigue}}$ in each layer. For the aggregates, the diffusion coefficients are set as zero.

### 3.3.4. Model Validation

Figure 8 shows the comparisons between the simulated results of the chloride profiles and chloride ion concentration obtained from the experimental tests on the beam specimens of B5, B6, B7, and B8. From Figure 8, in general, the chloride profiles within the concrete depth simulated by the 3D meso-scale model agree well with the experimental value for the B5, B6, B7, and B8 beam specimens. At a depth of 0 to 15 mm, the simulated results

and experimental results are almost identical. At depths between 15 mm and 30 mm, the simulated results have gaps with the experimental value. However, the difference in chloride concentration at the steel bar surface (nearly 40 mm depth) between the simulated results and experimental values is less than 19%. According to the study of Wu et al. [31] and Ghazy and Bassuoni [53], chloride exposure deteriorates the RC structures mainly by steel corrosion, and the steel corrosion is related to the chloride concentration on the steel bar. Hence, the model in this study is reliable for the assessment of RC beams.

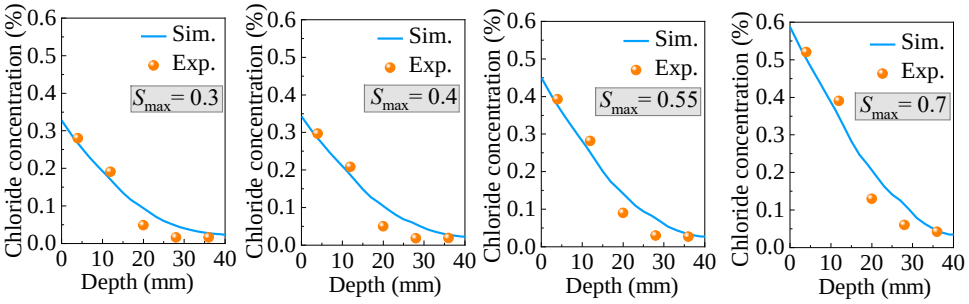


**Figure 8.** Simulated chloride concentration profiles and experimental chloride concentration data.

#### 3.3.5. Impact of Fatigue Loading on the Chloride Ingress into Concrete

The chloride ingress into concrete without and with fatigue stress after 0.5 years of chloride exposure is simulated by the above 3D meso-scale model to investigate the influence of fatigue stress on the chloride ingress, and the results are shown in Figure 9. To facilitate the display of chloride ingress, the bottom of the specimens is shown in Figure 9a, and the same approach is taken in the following study. For the concrete without fatigue stress, the diffusion coefficients in Section 3.3.3 are applied, and $C_s$ is taken as 0.3281%. For the concrete with fatigue stress, the diffusion coefficients in Section 3.3.3 are adopted, and the value of $C_s$ is referred to Table 3 for each stress level at the time of 0.5 years. Figure 9b indicates the remarkable influence of fatigue stress on the chloride diffusion depth and concentration in concrete. For the concrete without fatigue stress, the diffusion depth is almost 38 mm, i.e., the critical depth that the chloride concentration becomes constant and basically achieves the initial concentration. The diffusion depth is approximately 59 mm, 63 mm, 71 mm, and 75 mm for the concrete with the $S_{max}$ of 0.3, 0.4, 0.55, and 0.7, respectively. Meanwhile, at the concrete depth of 30 mm, the chloride concentration is 0.017% for the concrete without fatigue loading, while the concentration significantly increases to 0.038%, 0.041%, 0.054%, and 0.079%, respectively, for the concrete with the $S_{max}$ of 0.3, 0.4, 0.55, and 0.7. That is, the existence of fatigue stress generates at least a 124% increase in the chloride concentration at the depth of 30 mm in concrete. Thus, as a result of the concrete cracking and damage due to the fatigue stress [48], the existence of the fatigue stress and the increase in the fatigue stress significantly accelerate the chloride ion ingress into concrete.

#### 3.3.6. Impact of the Chloride Exposure Time on the Chloride Ingress into Fatigue-Damaged Concrete

In this section, the impact of the exposed time on chloride ingress into concrete is realized by a step-by-step method, aiming at considering the time-dependences of $C_s$ and $D_{un\text{-}cem}$. In this step-by-step method, 0.5 years is taken as one time step, and the results of one step depend on the results of its former step. That is, the final results considering different exposure times are obtained by the iteration of each time step. The $C_s$ and $D_{un\text{-}cem}$ are treated as constants in each time step. For example, for the cases of the simulation of 0.5 years of chloride exposure, $C_s$ is taken as 0.450%, and $D_{un\text{-}cem}$ is valued as $2.02 \times 10^{-12}$ ($m^2/s$), as listed in Table 3 and Figure 6. For the cases of the simulation of

1 year of chloride exposure, two steps are adopted. In the first step, $C_s$ is taken as 0.450%, and $D_{un\text{-}cem}$ is valued as 2.02 × $10^{-12}$ ($m^2$/s) with the exposure time of 0.5 years. In the second step, the initial conditions are the outcomes of the first step, where $C_s$ is taken as 0.450%, and $D_{un\text{-}cem}$ is taken as 1.63 × $10^{-12}$ ($m^2$/s) with the exposure time of 0.5 years. Hence, the chloride ingress within 1 year corresponds to the iteration of the above two steps. In addition, as shown in Figure 6, the $D_{un\text{-}cem}$ barely changes after 5 years; considering the palliation of the cement hydration and reactions between hydration products and chloride ions, the chloride diffusion coefficient is regarded as a constant after 5 years. Meanwhile, according to Guo et al. [43], $C_s$ can also be treated as a constant after 5 years.

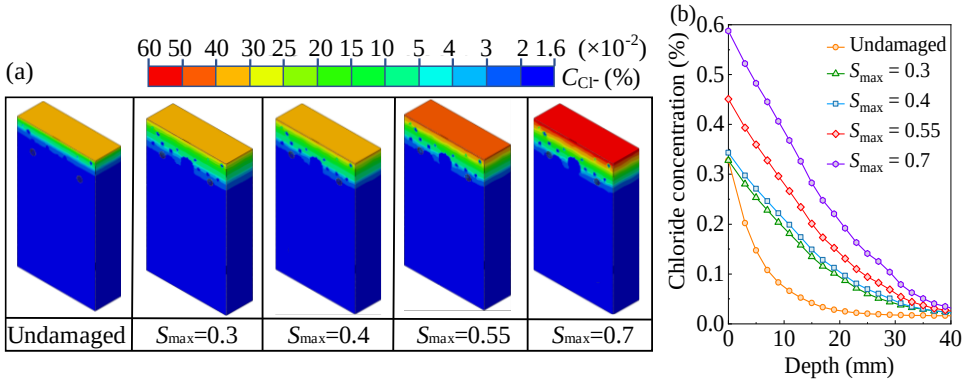


**Figure 9.** Chloride ingress in concrete with versus $S_{max}$: (**a**) chloride distribution in concrete and (**b**) chloride concentration profiles.

At a given stress level of 0.55, the chloride ingress distribution and the chloride concentration profile within 60 years of chloride exposure are presented in Figures 10 and 11, respectively. As the depth increases to 40 mm, the chloride concentration decreases from 0.45% to 0.027% (nearly 94.0% of the decrease) at the exposure time of 0.5 years, while the concentration decreases from 2.02% to 1.38% (decreasing 31.7%) as the exposure time extends to 20 years. However, the chloride concentration varies from 2.02% to 1.57% at 40 years of chloride exposure, and similarly, the chloride concentration varies from 2.02% to 1.67% at 60 years of exposure. The rate of chloride ingress into concrete tends to be slow after 40 years of chloride exposure, possibly caused by the decreasing gap between the chloride concentration at 40 mm depth and $C_s$.

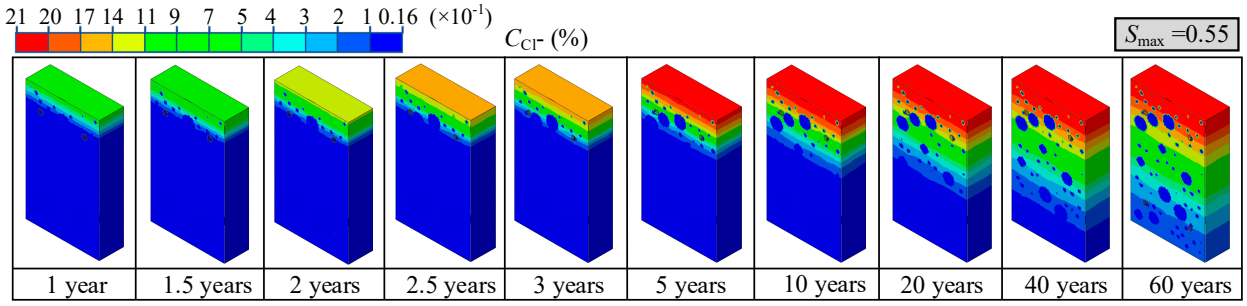


**Figure 10.** Chloride diffusion versus time of chloride exposure.

The concentration to generate the corrosion of the steel bar ($C_{crit}$), which is represented by the grey line in Figure 11, is valued at 0.69% based on the literature [54] in this study. As indicated in Figure 11, for the concrete with a stress level of 0.55, the time for the chloride concentration at the steel bar surface (40 mm depth) to reach the $C_{crit}$ is about 5 years. However, for the concrete without fatigue stress, the chloride concentration at the steel bar surface is 0.64% and 0.74% after 15 and 20 years of chloride exposure, respectively.

That is, for concrete without fatigue stress, the time of the corrosion generation is between 15 and 20 years. Hence, the corrosion generation time for the concrete without fatigue stress is over three times longer than that time with a stress level of 0.55.

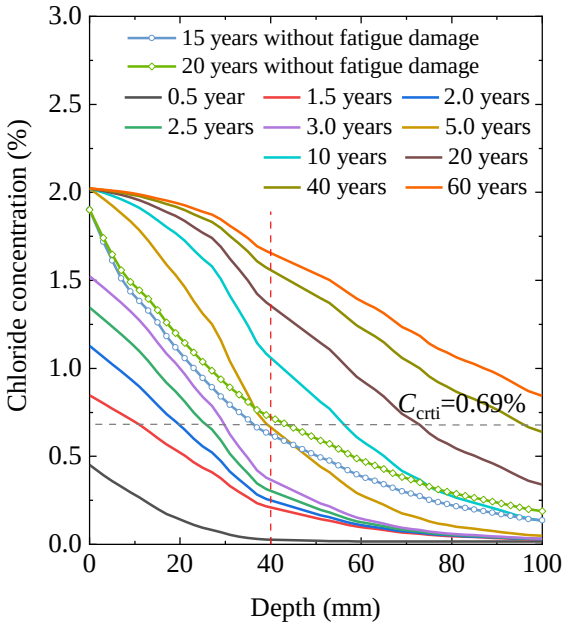


**Figure 11.** Chloride concentration profiles versus time of chloride exposure.

## 4. Validation and Application for the Deflection Prediction Model

### *4.1. Validation*

Based on the experimental results and Equation (30), the comparison of the experimental and calculated deflections of RC beams (A1–A4, B1, B3, and B4) is displayed in Table 4. The calculated deflections have a good agreement with the experimental deflection: the average value of $D_{exp}/D_{cal}$ is 1.18, and the coefficient of variation is 0.11, which verified the rationality of the model. In addition, the calculated value is about 18% higher than the experimental value, which is conservative and leaves a safe space for the development of structural deflection.

**Table 4.** Comparison of experimental and calculated deflection of RC beam.

| Beam | $N$ ($\times 10^6$) | $D_{exp}$ (mm) | $D_{cal}$ (mm) | $D_{exp}/D_{cal}$ | Beam | $N$ ($\times 10^6$) | $D_{exp}$ (mm) | $D_{cal}$ (mm) | $D_{exp}/D_{cal}$ |
|---|---|---|---|---|---|---|---|---|---|
| A1 | 10 | 1.55 | 1.62 | 1.05 | A2 | 10 | 1.85 | 2.42 | 1.33 |
| | 30 | 1.71 | 1.69 | 0.99 | | 30 | 2.10 | 2.52 | 1.20 |
| | 50 | 1.82 | 1.80 | 0.99 | | 50 | 2.21 | 2.66 | 1.20 |
| A3 | 10 | 2.38 | 3.24 | 1.36 | A4 | 3 | 2.78 | 3.74 | 1.35 |
| | 30 | 2.47 | 3.39 | 1.37 | | 5 | 3.11 | 3.81 | 1.23 |
| | 49 | 2.58 | 3.54 | 1.37 | | 9.7 | 3.17 | 4.05 | 1.28 |
| B1 | 10 | 1.64 | 1.73 | 1.05 | B3 | 9 | 2.52 | 3.27 | 1.30 |
| | 30 | 1.85 | 1.80 | 0.97 | | 18 | 2.76 | 3.39 | 1.23 |
| | 54 | 1.91 | 1.92 | 1.01 | | 27 | 2.85 | 3.54 | 1.24 |
| B4 | 3 | 3.31 | 3.77 | 1.14 | | | | | |
| | 5 | 3.49 | 3.87 | 1.11 | | | | | |
| | 7.7 | 3.63 | 4.06 | 1.12 | | | | | |

Note: $D_{exp}$ is the experimental deflection of the beam; $D_{cal}$ is the calculated deflection of the beam; the average value of $D_{exp}/D_{cal}$ is 1.18, and the coefficient of variation is 0.11.

*4.2. Prediction for Deflection of Fatigue-Damaged RC Beams After Chloride Exposure*

Based on Equation (25) and the simulation results of chloride attack, Figure 12 illustrates the combined effects of fatigue stress level and chloride exposure time on the deflection of RC beams. Figure 12a indicates that the mid-span deflection of the RC beams has a significant increment as the fatigue stress level. After 6 months of chloride exposure, the failure deflection at a stress level of 0.7 is 1.14, 1.53, and 2.26 times higher than that at stress levels of 0.55, 0.4, and 0.3, respectively, demonstrating an exponential growth trend. This reveals a markedly diminished influence of chloride exposure time on deflection compared to the fatigue stress level. As the exposure time increases from 5 to 60 years, the increase in failure deflection remains below 2.3%. This finding demonstrates that under long-term chloride exposure, the mechanical stress state remains the predominant factor governing structural deformation.

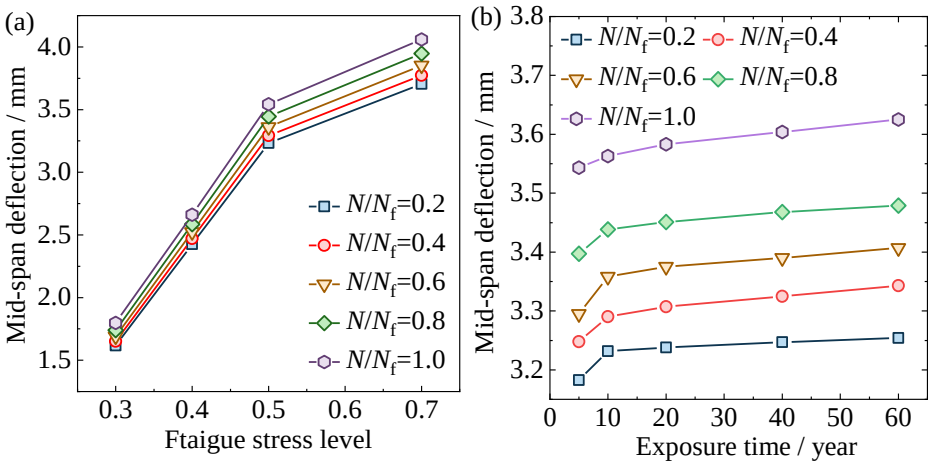


**Figure 12.** The mid-span deflection of RC beams: (**a**) effect of the fatigue stress level and (**b**) effect of the chloride exposure time.

## 5. Conclusions

In this study, 12 RC beam specimens were manufactured to investigate deflection variations under the combined effects of fatigue loading and chloride-induced corrosion. Based on the experimental results, a method for predicting deflection, which incorporates the effects of fatigue loading and pitting corrosion, was proposed. The corrosion rate of the steel bar is difficult to measure in practice; thus, it is obtained by numerical simulation. The main conclusions are as follows:

1. A deflection prediction model for RC beams under fatigue loading and pitting corrosion was developed and validated against the experimental data. The model comprehensively accounts for the number of fatigue cycles, fatigue stress level, degradation of concrete's elastic modulus, and the reduction in the steel cross-sectional area due to pitting corrosion.
2. A 3D meso-scale model is developed to conduct the chloride ingress analysis into the fatigue-damaged concrete, in which the effects of fatigue loading are considered by the accelerated and depth-dependent diffusion coefficients.
3. The existence of the fatigue stress generates at least a 124% increase in the chloride concentration at the depth of 30 mm in concrete, and the increasing fatigue stress significantly accelerates the chloride ingress into concrete. In addition, at the beginning of 20 years of chloride exposure, the chloride concentration along the concrete depth decreases obviously, at least 31.7%. After 40 years of exposure, the concentration within the 40 mm depth becomes steady. The fatigue stress level of 0.55 decreases the

corrosion generation time of the steel bar at least 10 years compared with the concrete without fatigue stress.

4. Based on the deflection prediction model and simulated results, it can be found that under long-term erosion conditions, the mechanical stress state remains the dominant factor controlling structural deformation development. The increase in deflection of RC beams is less than 2.3% with the exposure time increasing from 5 years to 60 years, while the increment is more than 125.8% with the fatigue stress level increasing from 0.3 to 0.7.

Extending the service life of reinforced concrete structures is a practical and vital strategy for enhancing sustainability, as it directly curtails the resource consumption and carbon emissions from repair and reconstruction. To support this goal, this study has developed a deflection prediction method that accounts for the combined effects of fatigue loading and pitting corrosion, providing a tool for more accurate durability assessments. It should be noted that the experimental validation and the proposed model in this study are based on RC beams with a specific geometry and concrete mixture. Consequently, the direct applicability of the findings is constrained within the investigated ranges of fatigue stress levels and reinforcement ratios. Future research is recommended to incorporate a wider spectrum of parameters, such as varying beam dimensions, concrete strengths, and reinforcement configurations, to further generalize and validate the proposed methodology. Meanwhile, the current model does not include an explicit formulation for the degradation of bond–slip between the steel reinforcement and concrete due to corrosion. This simplification is based on the experimental observations in this study, where the failure mode was governed by steel fracture or concrete crushing rather than bond failure, and on the satisfactory agreement of deflection predictions achieved by focusing on the dominant factors of cross-sectional area loss and material property degradation. Future refinement of the model could incorporate bond–slip effects for a more comprehensive simulation.

**Author Contributions:** Conceptualization, J.Y. and J.W.; methodology, J.Y.; software, J.Y.; validation, J.Y., J.W. and L.J.; formal analysis, J.Y.; investigation, J.Y.; re-sources, L.J. and X.D.; data curation, J.W.; writing—original draft preparation, J.Y.; writing—review and editing, J.Y.; visualization, J.W. and X.D.; supervision, J.W. and X.D.; project administration, X.D.; funding acquisition, J.W. and L.J. All authors have read and agreed to the published version of the manuscript.

**Funding:** This work was supported by the National Natural Science Foundation of China (Grant No. 52478114) and the Beijing Natural Science Foundation (Grant No. JQ22025). Jieqiong Wu and Liu Jin are the corresponding principal investigators for these grants, respectively.

**Data Availability Statement:** The original contributions presented in this study are included in the article. Further inquiries can be directed to the corresponding author.

**Acknowledgments:** This research was financially supported by the National Natural Science Foundation of China (No. 52478114) and the Beijing Natural Science Foundation (No. JQ22025). The support is gratefully acknowledged.

**Conflicts of Interest:** The authors declare no conflicts of interest.

## References

1. Fu, Z.Q.; Ji, B.H.; Ye, Z.; Wang, Y.X. Fatigue Evaluation of Cable-stayed Bridge Steel Deck Based on Predicted Traffic Flow Growth. *KSCE J. Civ. Eng.* **2017**, *21*, 1400–1409. [CrossRef]
2. Liu, Q.F.; Hu, Z.; Wang, X.E.; Zhao, H.T.; Qian, K.; Li, L.J.; Meng, Z. Numerical study on cracking and its effect on chloride transport in concrete subjected to external load. *Constr. Build. Mater.* **2022**, *325*, 126797. [CrossRef]
3. Otieno, M. Sensitivity of chloride-induced corrosion rate of steel in concrete to cover depth, crack width and concrete quality. *Mater. Struct.* **2017**, *50*, 9. [CrossRef]
4. *GB/T 50476-2019*; Standard for Design of Concrete Structure Durability. China Architecture & Building Press: Beijing, China, 2019.

5. American Concrete Institute. *Building Code Requirements for Reinforced Concrete: ACI-318*; ACI: Farmington Hills, MI, USA, 1989.
6. Wang, B.; Huang, Q.; Liu, X.L.; Ding, Y. Study on stiffness deterioration in steel-concrete composite beams under fatigue loading. *Steel Compos. Struct.* **2020**, *34*, 499–509.
7. Zuo, X.D.; Ni, Y.S.; Zhang, J.Q.; Zhao, S.C. Influences of fatigue stiffness degradation of in-service concrete T-beams on natural vibration frequency. *J. Asian Archit. Build. Eng.* **2023**, *24*, 1176–1185. [CrossRef]
8. Li, X.; Zhang, J.W.; Cheng, J. Study on the stiffness degradation in concrete continuous beam with externally prestressed CFRP tendons under fatigue loading. *Adv. Struct. Eng.* **2021**, *24*, 2119–2130. [CrossRef]
9. Eljufout, T.; Toutanji, H. Prediction of deflection progression of RC beams strengthened with NSM FRP composites. In Proceedings of the International Conference on Fibre-Reinforced Polymer (FRP) Composites in Civil Engineering, Istanbul, Turkey, 8–10 December 2021; Springer: Berlin/Heidelberg, Germany, 2021; pp. 1505–1517.
10. Atutis, E.; Valivonis, J.; Atutis, M. Deflection determination method for BFRP prestressed concrete beams under fatigue loading. *Compos. Struct.* **2019**, *226*, 111182. [CrossRef]
11. Zhu, W.; François, R.; Coronelli, D.; Cleland, D. Effect of corrosion of reinforcement on the mechanical behaviour of highly corroded RC beams. *Eng. Struct.* **2013**, *56*, 544–554. [CrossRef]
12. Zhang, K.; Zhang, J.; Jin, W.; Mao, J.; Long, J. Stiffness degradation for fatigue of reinforced concrete beams after electrochemical rehabilitation. *Constr. Build. Mater.* **2020**, *260*, 120455. [CrossRef]
13. Huang, Y.; Wei, J.; Dong, R. Stiffness of corroded partially prestressed concrete T-beams under fatigue loading. *Mag. Concr. Res.* **2019**, *72*, 325–338. [CrossRef]
14. Zhang, T.; Cui, X.; Li, P.; Li, X.; Wang, S.; Zhang, C. Stiffness degradation analysis of reinforced concrete beams under corrosion-fatigue coupling action based on experimental research. *Structures* **2023**, *54*, 1278–1298. [CrossRef]
15. Dackman, D.; Berrocal, C.G.; Rempling, R.; Fernandez, I. A framework for evaluating steel loss from the evolution of corrosion-induced deflections in reinforced concrete beams with non-uniform reinforcement corrosion. *Eng. Struct.* **2024**, *317*, 118593. [CrossRef]
16. Yuan, Y.S.; Ji, Y.S.; Shah, S.P. Comparison of two accelerated corrosion techniques for concrete structures. *ACI Struct. J.* **2007**, *104*, 344–347. [CrossRef]
17. Dasar, A.; Hamada, H.; Sagawa, Y.; Yamamoto, D. Deterioration progress and performance reduction of 40-year-old reinforced concrete beams in natural corrosion environments. *Constr. Build. Mater.* **2017**, *149*, 690–704. [CrossRef]
18. Chen, J.W.; Fu, C.Q.; Ye, H.L.; Jin, X.Y. Corrosion of steel embedded in mortar and concrete under different electrolytic accelerated corrosion methods. *Constr. Build. Mater.* **2020**, *241*, 117971. [CrossRef]
19. Hu, P.; Meng, Q.C.; Hu, W.P.; Shen, F.; Zhan, Z.X.; Sun, L.L. A continuum damage mechanics approach coupled with an improved pit evolution model for the corrosion fatigue of aluminum alloy. *Corros. Sci.* **2016**, *113*, 78–90. [CrossRef]
20. Muthulingam, S.; Rao, B.N. Non-uniform time-to-corrosion initiation in steel reinforced concrete under chloride environment. *Corros. Sci.* **2014**, *82*, 304–315. [CrossRef]
21. Zhao, P.; Xu, G.; Wang, Q.; Zeng, Z. Corrosion behavior of steel bars in simulated concrete pore solution under the coupling action of chloride salt and DC stray current. *Constr. Build. Mater.* **2024**, *455*, 139126. [CrossRef]
22. Tian, Z.; Kang, X.; Ji, H.; Ye, H. Quantitative relationship between microstructure of steel-concrete interface and chloride-induced corrosion rate of steel in unsaturated cementitious materials. *Cem. Concr. Res.* **2025**, *188*, 107736. [CrossRef]
23. Oh, B.H.; Jang, S.Y. Prediction of diffusivity of concrete based on simple analytic equations. *Cem. Concr. Res.* **2004**, *34*, 463–480. [CrossRef]
24. Du, X.; Jin, L.; Ma, G. A meso-scale numerical method for the simulation of chloride diffusivity in concrete. *Finite Elem. Anal. Des.* **2014**, *85*, 87–100. [CrossRef]
25. Xu, J.; Li, F. A meso-scale model for analyzing the chloride diffusion of concrete subjected to external stress. *Constr. Build. Mater.* **2017**, *130*, 11–21. [CrossRef]
26. Wu, J.; Zhang, R.; Diao, B.; Zhang, W.; Xu, J. Effects of pre-fatigue damage on high-cycle fatigue behavior and chloride permeability of RC beams. *Int. J. Fatigue* **2019**, *122*, 9–18. [CrossRef]
27. Wu, J.Q.; Diao, B.; Xu, J.C.; Zhang, R.X.; Zhang, W.M. Effects of the reinforcement ratio and chloride corrosion on the fatigue behavior of RC beams. *Int. J. Fatigue* **2020**, *131*, 105299. [CrossRef]
28. Wu, J.Q.; Xu, J.C.; Diao, B.; Panesar, D.K. Impacts of reinforcement ratio and fatigue load level on the chloride ingress and service life estimating of fatigue loaded reinforced concrete (RC) beams. *Constr. Build. Mater.* **2021**, *266*, 120999. [CrossRef]
29. Wu, J.Q.; Xu, J.C.; Diao, B.; Panesar, D.K. Chloride Diffusivity, Fatigue Life, and Service Life Analysis of RC Beams under Chloride Exposure. *J. Mater. Civ. Eng.* **2020**, *32*, 04020107. [CrossRef]
30. Wu, J.Q.; Diao, B.; Cao, Y.; Zhong, J.; Shi, X.M. Chloride concentration distributions in fatigue damaged RC beams revealed by energy-dispersive X-ray spectroscopy. *Constr. Build. Mater.* **2020**, *234*, 117396. [CrossRef]
31. Wu, J.Q.; Yang, J.; Zhang, R.B.; Jin, L.; Du, X.L. Fatigue life estimating for chloride attacked RC beams using the S-N curve combined with mesoscale simulation of chloride ingress. *Int. J. Fatigue* **2022**, *158*, 106751. [CrossRef]

32. Li, C.; Wu, M.X.; Chen, Q.; Jiang, Z.W. Chemical and mineralogical alterations of concrete subjected to chemical attacks in complex underground tunnel environments during 20-36 years. *Cem. Concr. Compos.* **2018**, *86*, 139–159. [CrossRef]
33. *GB50010-2010*; Code for Design of Concrete Structures. China Architecture & Building Press: Beijing, China, 2010.
34. Sun, J.; Ding, Z.; Huang, Q. Development of EIFS-based corrosion fatigue life prediction approach for corroded RC beams. *Eng. Fract. Mech.* **2019**, *209*, 1–16. [CrossRef]
35. Wu, J.; Xu, J.; Diao, B.; Jin, L.; Du, X. Fatigue life prediction for the reinforced concrete (RC) beams under the actions of chloride attack and fatigue. *Eng. Struct.* **2021**, *242*, 112543. [CrossRef]
36. Stewart, M.G.; Al-Harthy, A. Pitting corrosion and structural reliability of corroding RC structures: Experimental data and probabilistic analysis. *Reliab. Eng. Syst. Saf.* **2008**, *93*, 373–382. [CrossRef]
37. Val, D.V.; Melchers, R.E. Reliability of deteriorating RC slab bridges. *J. Struct. Eng. ASCE* **1997**, *123*, 1638–1644. [CrossRef]
38. Wu, J.; Guo, L.; Jin, L.; Du, X. Tests on adhesion properties of non-uniformly corroded steel-concrete reinforcement. *J. Harbin Inst. Technol.* **2022**, *54*, 109–117. (In Chinese)
39. Wu, J.; Zhang, X.; Guo, L.; Jin, L.; Du, X. Probabilistic bond strength prediction between the corroded reinforcing bars and concrete considering the concrete strength and non-uniform corrosion. *Constr. Build. Mater.* **2022**, *357*, 129338. [CrossRef]
40. Ove, H.J. Fatigue of concrete by constant and variable amplitude loading. *ACI Spec. Publ.* **1982**, *75*, 71–110.
41. Jiang, Z.L.; Qian, Z.W.; Gu, X.L.; Zhu, J.H.; Long, W.J.; Xing, F. Statistical analysis of chloride concentration distribution in concrete by a meso-scale model considering irregular shape aggregates. *Constr. Build. Mater.* **2022**, *319*, 126143. [CrossRef]
42. Song, H.W.; Lee, C.H.; Ann, K.Y. Factors influencing chloride transport in concrete structures exposed to marine environments. *Cem. Concr. Compos.* **2008**, *30*, 113–121. [CrossRef]
43. Guo, Z.W.; Guo, R.Q.; Yao, G.W. Multi-factor model to predict surface chloride concentration of concrete based on fuzzy logic system. *Case Stud. Constr. Mater.* **2022**, *17*, e01305. [CrossRef]
44. Sun, G.W.; Sun, W.; Zhang, Y.S.; Liu, Z.Y. Multi-scale Modeling of the Effective Chloride Ion Diffusion Coefficient in Cement-based Composite Materials. *J. Wuhan Univ. Technol.-Mater. Sci. Ed.* **2012**, *27*, 364–373. [CrossRef]
45. *GB/T 21650.1*; Pore Size Distribution and Porosity of Solid Materials by Mercury Porosimetry and Gas Adsorption. Standards Press of China: Beijing, China, 2008.
46. *ASTMA C138/C138M-17a*; Standard Test Method for Density (Unit Weight), Yield, and Air Content (Gravimetric) of Concrete. ASTM International: West Conshohocken, PA, USA, 2017.
47. Amey, S.; Geiker, M.; Manning, D.; Archibald, J.; Hookham, C.; Mukherjee, P.; Buenfeld, N.R.; Irwin, W.J.; Pommersheim, J.; Cady, P.D.; et al. *Service-Life Prediction—State-of-the-Art Report*; ACI Committee 365: Farmington Hills, MI, USA, 2000.
48. Kim, J.; Hong, G.; Oh, S.; Choi, S. Application of various fractal models in characterizing the morphology of pore structures of hydrating cement pastes. *J. Mater. Res. Technol.* **2022**, *20*, 3818–3835. [CrossRef]
49. Jin, W.; Yuan, Y.; Wei, J.; Wang, H. *Durability Theory and Design Method of Concrete Structure Under Chloride Environment*; Science Press: Beijing, China, 2011.
50. Liu, Q.F.; Xia, J.; Easterbrook, D.; Yang, J.; Li, L.Y. Three-phase modelling of electrochemical chloride removal from corroded steel-reinforced concrete. *Constr. Build. Mater.* **2014**, *70*, 410–427. [CrossRef]
51. Shen, J.S.; Liu, J.Z.; Xu, Y.D.; Jia, K.H.; Wu, F.Y.; Chen, W.; Zhu, D. Corrosion Cracking Process of Reinforced Concrete under the Coupled Effects of Chloride and Fatigue Loading. *KSCE J. Civ. Eng.* **2021**, *25*, 3376–3389. [CrossRef]
52. Shayanfar, M.; Farnia, S.; Ghanooni-Bagha, M.; Massoudi, M. The effect of crack width on chloride threshold reaching time in reinforced concrete members. *Asian J. Civ. Eng.* **2020**, *21*, 625–637. [CrossRef]
53. Ghazy, A.; Bassuoni, M.T. Resistance of concrete to different exposures with chloride-based salts. *Cem. Concr. Res.* **2017**, *101*, 144–158. [CrossRef]
54. Song, H.W.; Pack, S.W.; Ann, K.Y. Probabilistic assessment to predict the time to corrosion of steel in reinforced concrete tunnel box exposed to sea water. *Constr. Build. Mater.* **2009**, *23*, 3270–3278. [CrossRef]


**Disclaimer/Publisher's Note:** The statements, opinions and data contained in all publications are solely those of the individual author(s) and contributor(s) and not of MDPI and/or the editor(s). MDPI and/or the editor(s) disclaim responsibility for any injury to people or property resulting from any ideas, methods, instructions or products referred to in the content.